Magnetic properties of ultrafine $MnFe_2O_4$ powders prepared by mechanochemical processing

M. Muroi, R. Street, and P. G. McCormick
Research Centre for Advanced Mineral and Material Processing, Department of Physics, The University of Western Australia, Nedlands, Western Australia 6907, Australia

J. Amighian
Department of Physics, Isfahan University, Isfahan 81744, Iran

(Received 1 September 2000; revised manuscript received 18 December 2000; published 18 April 2001)

Ultrafine $MnFe_2O_4$ powders have been synthesized via the displacement reaction $2FeCl_3+4MnO \rightarrow MnFe_2O_4+3MnCl_2$ activated by high-energy ball milling. Single-phase $MnFe_2O_4$ powders having crystallite sizes ranging between 9.5 and 40 nm have been obtained after removing the by-product ($MnCl_2$) and unreacted ($FeCl_3$ and MnO) phases from the as-milled or annealed powders by washing and magnetic separation. Magnetic measurements show that the spontaneous magnetization decreases with crystallite size; that the coercivity increases with decreasing temperature; and that below about 50 K the temperature dependence of coercivity becomes very strong, and the hysteresis loop becomes asymmetric with the remanent magnetization and the coercivity both enhanced in the upper branch when the sample is cooled in the maximum field. These observations are discussed in terms of a model in which it is assumed that each crystallite consists of a ferrimagnetic core surrounded by a spin-glass shell and the spins in the core and shell are exchange coupled.

DOI: 10.1103/PhysRevB.63.184414 PACS number(s): 75.50.Tt, 75.50.Gg, 75.60.Ej

I. INTRODUCTION

Spinel ferrites have been studied for more than 50 years from both scientific and technological points of view. On the one hand, they are widely used for components in high-frequency electronic devices, taking advantage of their high initial permeability and high resistivity; accordingly, a major focus of the research effort has been the development of materials and fabrication processes leading to better performances. On the other hand, spinel ferrites exhibit a rich variety of magnetic properties, reflecting the flexibility of the spinel structure in accommodating a wide range of cations, which are of great fundamental interest in their own right. Among the various topics in fundamental research on spinel ferrites, the magnetic properties of ultrafine particles have recently attracted considerable attention.

Ultrafine powders of a range of spinel ferrites have been prepared and their properties extensively studied.[1–17] In most of these studies, the powders were synthesized by wet chemical methods, e.g., coprecipitation,[1–6] and it has been reported that they exhibit magnetic properties different from those of bulk samples prepared by standard ceramic processing. Examples include reduced spontaneous magnetizations (M_s),[1–4] enhanced or reduced Curie temperatures (T_c),[3,4] and spin canting as revealed by Mössbauer spectroscopy.[2,5] It has also been argued that the cation distribution among the A and B sites in $MnFe_2O_4$ nanopowders prepared by coprecipitation depends on the crystallite size,[4,6–9] which has aroused a great deal of controversy over the origin of the crystallite size dependence of T_c.[3,4,7–9] Another method of preparing ferrite nanopowders is mechanical grinding of coarse powders.[10–12,14] It has been shown that $NiFe_2O_4$ nanopowders thus prepared exhibit displaced hysteresis loops with irreversibility persisting up to 160 kOe at low temperatures.[10–12] This behavior has been discussed in terms of exchange coupling between the ferrimagentic core and the spin-glass surface layer.[11–13] The preparation of spinel ferrites by other methods, such as mechanical alloying[15,16] and combustion in urea,[17] has also been reported but their magnetic properties have not been investigated in depth.

In the present work, we have synthesized $MnFe_2O_4$ powders having crystallite sizes in the range between 9.5 and 40 nm by mechanochemical processing (MCP), a process that makes use of chemical reactions activated by high-energy ball milling. Extensive magnetic measurements have revealed various features characteristic of exchange-coupled systems,[18] e.g., strong temperature dependence of coercivity (H_c) and displaced field-cooled (FC) hysteresis loops at low temperatures. These observations, as well as reductions in M_s with decreasing crystallite size, are mostly consistent with earlier results[2–4,10–12] and are discussed in terms of the core-shell exchange-coupling model proposed by Kodama and co-workers.[11–13] Other discoveries include enhancement of remanent magnetization (M_r) in the upper branch of the FC hysteresis loop and gradual decreases in H_c and M_r as the hysteresis loop measurement is repeated at low temperature. Explanations of these observations are provided within the framework of the core-shell exchange-coupling model.[11–13] The difference between MCP and wet-chemical methods is also discussed.

II. EXPERIMENTAL PROCEDURE

$MnFe_2O_4$ powders have been prepared by MCP. The starting materials used were $FeCl_3$ and MnO mixed in the ratio appropriate for the reaction

$$2FeCl_3+4MnO \rightarrow MnFe_2O_4+3MnCl_2. \quad (1)$$

A total of 4 g of the powder, together with seven 12.6-mm hardened-steel balls, was loaded in a hardened-steel vial in an Ar-filled glove box and milled for 24 h in a Spex 8000 mixer/mill. The milled powder was annealed at temperatures

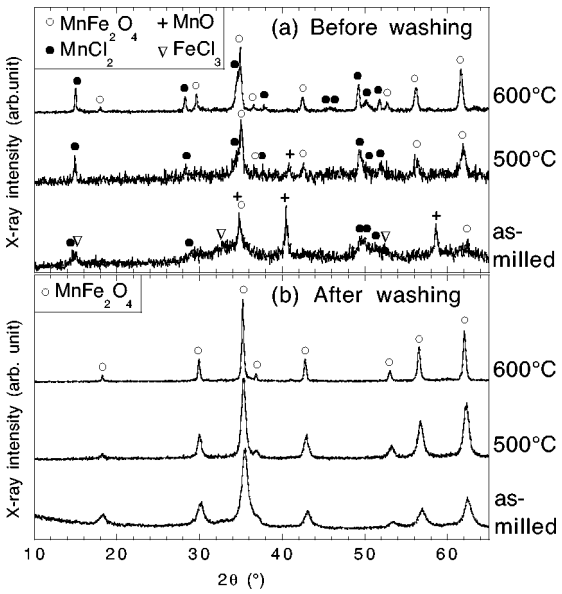

FIG. 1. XRD spectra for the as-milled and annealed powders (a) before and (b) after washing.

up to 600 °C in Ar for 1 h. After annealing, the powder was washed several times with deionized water; during the washing procedure, only those particles that were magnetic at room temperature were collected by means of magnetic separation, while the compounds dissolved in water and nonmagnetic particles in suspension were discarded.

The crystal structure was determined by x-ray diffraction (XRD), and the particle morphology was examined by transmission electron microscopy (TEM). Magnetic measurements were made using a superconducting quantum interference device magnetometer on cold-pressed pellets 5 mm in diameter and about 0.5 mm in thickness. The magnetic field was applied parallel to the flat surface of the pellet to reduce demagnetizing effects.

III. RESULTS AND DISCUSSION

In Fig. 1(a), XRD spectra for the as-milled and annealed powders are shown. The peaks in the spectrum for the as-milled powder correspond to $FeCl_3$, MnO, $MnFe_2O_4$, and $MnCl_2$, indicating that reaction (1) partly occurred during milling. As the annealing temperature (T_a) increases, the relative intensities of the $FeCl_3$ and MnO peaks decrease, and at $T_a = 600$ °C $MnFe_2O_4$ and $MnCl_2$ are the only remaining phases. After washing, single-phase $MnFe_2O_4$ was obtained from both the as-milled and annealed powders, as can be seen in the XRD spectra presented in Fig. 1(b).

In Fig. 2 the crystallite size (D), calculated from XRD peak broadening using Scherrer's formula, is plotted as a function of T_a. It can be seen that D increases with T_a, slowly up to 500 °C and then at an accelerated rate above 500 °C.

TEM photographs of the as-milled powder (after washing) are shown in Fig. 3. The powder consists of equiaxed particles mostly in the range 5–20 nm in size, consistent with D determined from the XRD data, 9.5 nm. Reasonable agreement of the particle size determined by TEM examination with D was confirmed also for the annealed powders.

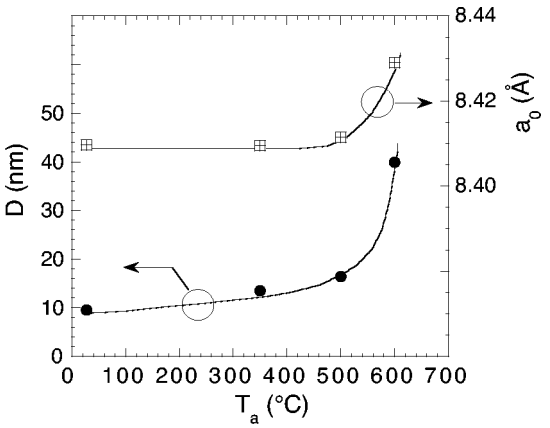

FIG. 2. Variations with annealing temperature (T_a) of the crystallite size (D) and the lattice constant (a_0).

The variation of the lattice constant (a_0) with T_a is included in Fig. 2. It can be seen that a_0 is smaller than the value for bulk $MnFe_2O_4$, 8.51 Å,[19] and tends to decrease as T_a, and hence D, decrease. A similar decrease in a_0 with decreasing particle size has been observed in $Mn_{0.6}Co_{0.4}Fe_2O_4$ prepared by coprecipitation.[1]

Room-temperature hysteresis loops for the washed powders are shown in Fig. 4. They are typical of soft ferromagnets; however, complete magnetic saturation is not achieved even at 50 kOe. The spontaneous magnetization (M_s) is smaller than the value for bulk $MnFe_2O_4$, 80 emu/g,[19] and decreases with D, suggesting the presence of a surface region (shell) with a reduced magnetization (M). (M_s is defined here as the intercept at $H=0$ of the straight line obtained by linear fit to the data points for $H \geqslant 30$ kOe.) We can estimate the shell thickness (t), assuming that t is independent of D and $M=0$ for the shell. The variation of M_s with D will then be described by $M_s = M_{s0}(D-2t)^3/D^3$, or $M_s^{1/3} = M_{s0}^{1/3}(1-2t/D)$, where M_{s0} is the M_s of bulk $MnFe_2O_4$. As can be seen in the inset of Fig. 4, $M_s^{1/3}$ and $1/D$ indeed show a good linear relationship, and from a linear fit to the data points M_{s0} and t were estimated at 78.1 emu/g and 9.1 Å, respectively. (The intercept at $1/D=0$ and the slope of the straight line correspond to $M_{s0}^{1/3}$ and $2tM_{s0}^{1/3}$, respectively.) M_{s0} thus

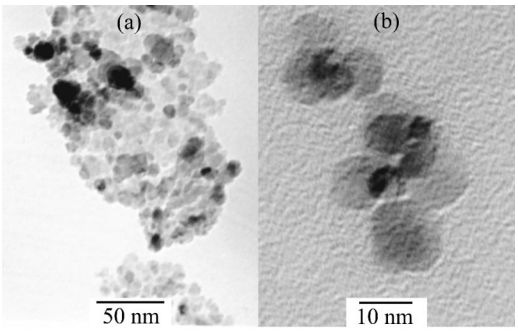

FIG. 3. TEM photographs of the as-milled powder (washed). The powder contains large agglomerates (a), which are easily broken up by agitation in an ultrasonic bath (b).

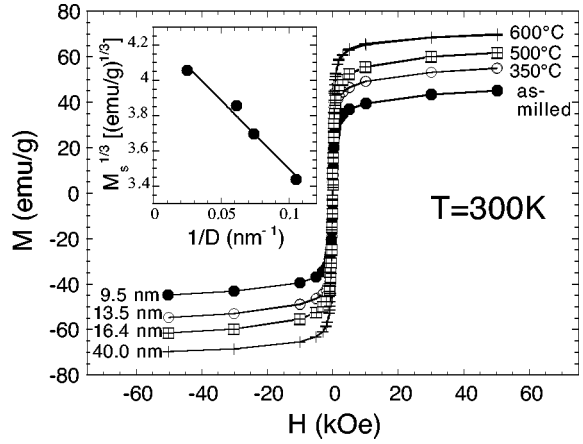

FIG. 4. Hysteresis loops measured at 300 K for the powders having various crystallite sizes. Inset: $M_s^{1/3}$ vs $1/D$ plot, where M_s is the spontaneous magnetization and D is the crystallite size.

obtained is close to the value for bulk $MnFe_2O_4$, 80 emu/g, whereas t is comparable to the lattice constant (≈ 8.5 Å). The estimated value of t is somewhat larger than that obtained by Tang *et al.*[3] from a similar analysis (7 Å),[20] but it is smaller than the values estimated from Mössbauer measurements on $CoFe_2O_4$ nanoparticles (10–16 Å).[5] The latter discrepancy is due largely to the difference in the assumptions concerning the contribution to M_s from the shell: in our estimation, $M_s = 0$ was assumed for the shell whereas in Ref. 5 random spin-canting angles between 0° and 90° were assumed for the spins in the shell, corresponding to $M_s = M_{s0}/2$ for the shell. [A more likely spin configuration in the shell is one in which the spins are almost random ($M = 0$) at the surface and gradually recovers a collinear ferrimagnetic arrangement ($M = M_s$) with increasing distance form the surface.[21]]

Two interpretations have been provided regarding the magnetic structure of the shell: (i) the shell is weakly magnetic and noninteracting[3] and (ii) the shell consists of disordered spins coupled through frustrated exchange interactions.[11–13] The first interpretation, however, is inconsistent with the magnetization (M) vs temperature (T) curves displayed in Fig. 5(a), which show little variation in M with T in the low-temperature region; if the spins were noninteracting, M would increase sharply at the lowest temperature. (Note that the measurement on the 9.5-nm powder, in which the fraction of the spins in the shell is as large as 26%, was made down to 1.8 K.) Furthermore, the M vs T curve measured in a low field of 10 Oe [Fig. 5(c)] exhibits a steep decrease in M at about 50 K, a clear indication of spin freezing. Thus, the second interpretation is more reasonable, that is, the shell is well described as a spin glass.[11–13]

The existence of spin-glass shells in ferrite nanoparticles has been explained in terms of broken exchange bonds at the surface and surface anisotropy.[2,11–13] In many spinel ferrites, strong antiferromagnetic *A-B* exchange interactions dominate weaker, competing *A-A* and *B-B* exchange interactions, leading to a ferrimagnetic configuration in which the spins on the *A* and *B* sites are antiparallel. At the surface, however, the cations have various numbers of neighboring cations on

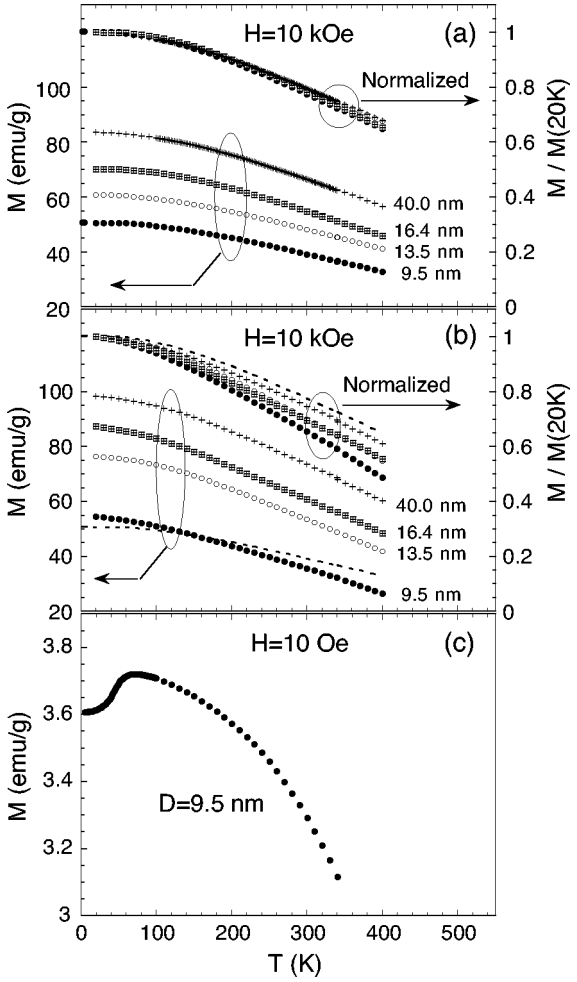

FIG. 5. (a) Field-cooled magnetization (M) vs temperature (T) curves measured in a field of 10 kOe for the powders having various crystallite sizes. The curves normalized to the values at 20 K are also shown. (b) Field-cooled M vs T curves measured in a field of 10 kOe for the powders subjected to additional annealing at 480 °C. The dashed lines are the M vs T curves for the 9.5-nm powder before the additional annealing. (c) Field-cooled M vs T curve measured in a field of 10 Oe for the 9.5-nm powder.

the two sublattices. Some of the exchange bonds are thus broken, resulting in a distribution of net exchange fields and hence spin canting at various angles from the net moment. In addition, asymmetric oxygen coordination at surface-cation sites causes large perturbations to the crystal field, resulting in surface anisotropy;[12,13] the easy axis is defined by the dipole moment of the neighboring ions and is hence approximately radial.[12,13]

Although the above model provides a satisfactory explanation of the presence of the magnetically disordered shell, it alone is not sufficient to account for the shell thickness. Numerical calculations incorporating the above effects[11–13] indicate that the shell is very thin with a collinear spin configuration recovered within an atomic layer or two, whereas the thickness of the shell determined experimentally is comparable to or greater than the lattice constant. We suggest that asymmetric atomic arrangement at the surface results in imbalance of the exchange interactions, and in approxi-

mately radial uniaxial anisotropy, for the cations not only at, but also near the surface through long-range Coulomb interactions. Deep inside a crystal, the electrostatic potential or the Madelung potential is essentially the same for all crystallographically equivalent sites and so are the on-site Coulomb energy (U) and the charge-transfer energy (Δ). (In ionic crystals, U and Δ are determined largely by the ionization potential and the Madelung potential at the relevant atomic site.[22]) Therefore, the exchange interactions, which in general are functions of U, Δ, and the hopping integral, are also the same for equivalent cation pairs. Near the surface, however, the Madelung potential is different from that deep inside the bulk, since there are no ions outside the crystal that contribute to the Madelung potential. U and Δ, and hence J, will thus vary even among crystallographically equivalent cation pairs, resulting in a distribution of exchange fields and hence magnetic disorder. This effect diminishes only gradually with increasing distance from the surface because of the long-range nature of Coulomb interactions. The perturbations to the crystal field are not limited to the surface cations either. Although a crystal is electrically neutral as a whole, charge neutrality is not necessarily satisfied for each crystallographic plane. A charged surface layer creates a roughly radial electric field, and hence approximately radial, uniaxial anisotropy at a cation site *near* the surface.

It is observed in Fig. 5(a) that the M vs T curve shifts downward as D decreases, consistent with the decrease in M_s with D (Fig. 4). When normalized, however, the four curves collapse into a single curve. This implies that the four samples have approximately the same cation distributions among the A and B sites. (It is well established that as the degree of inversion increases, the low-temperature magnetization decreases and T_c increases leading to a weaker T dependence of M.[23]) In the case of $MnFe_2O_4$ powders prepared by wet-chemical methods, by contrast, the degree of inversion has been claimed to increase with decreasing particle size.[4,7–9] This difference is possibly related to the oxidation of Mn^{2+} to Mn^{3+}, which is known to have a strong influence on the cation distribution.[4,9] In wet-chemical methods, the spinel phase is formed in an aqueous solution, allowing the oxidation of Mn^{2+} to Mn^{3+} during crystal growth. In the case of MCP, on the other hand, the oxidation of Mn will not occur during crystal growth, since it is a dry process in a closed container and the net cation valence is conserved. Mn^{2+} ions on the B site may be oxidized during washing, drying, and subsequent handling in air, but it will be limited to the surface layer, which does not contribute much to the net magnetization. With less complication arising from the particle-size dependence of inversion, the powders prepared by MCP are suitable for the study of intrinsic size effects on the magnetic properties.[24]

The above argument is further supported by the data presented in Fig. 5(b), where the M vs T curves are shown for the samples subjected to additional annealing at 480 °C in Ar for 20 min. It can be seen that the M vs T curves exhibit stronger temperature dependence and greater low-temperature magnetizations as compared with those in Fig. 5(a). [For comparison, the M vs T curve before the additional annealing is replotted in Fig. 5(b) (dashed lines) for the 9.5-nm powder.] The normalized curve is now clearly dependent on D with stronger temperature dependence for a smaller D. (XRD measurements on the samples before and after annealing have shown no evidence of grain growth.) These data strongly suggest that the degree of inversion has decreased during the additional annealing and that the decrease is more significant the smaller the crystallite size. Note that two of the four powders were annealed at higher temperatures (500 °C and 600 °C) for a longer period (1 h) prior to washing and yet the four as-washed powders exhibit essentially the same temperature dependence of M [Fig. 5(a)]. We explain these observations in terms of defect-assisted cation diffusion. Exposure of the samples to air and water during washing allows oxidation of Mn^{2+} near the surface to Mn^{3+}, which results in the formation of cation vacancies because of the charge-neutrality condition. These cation vacancies will facilitate cation redistribution during subsequent annealing. Because of the larger surface area, the smaller particles will have a greater fraction of Mn^{3+} ions and hence a higher vacancy concentration, thus making cation redistribution easier. On the other hand, the Mn ions cannot be oxidized during initial annealing prior to washing, since the net cation valence is conserved at this stage as already mentioned. The vacancy concentration in the $MnFe_2O_4$ phase is low, as a result, making cation redistribution difficult.[25]

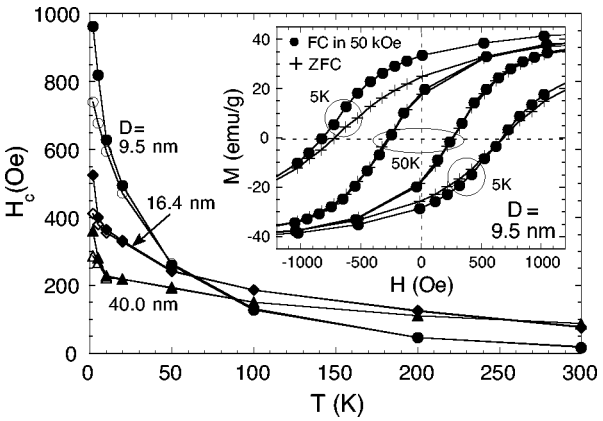

FIG. 6. Variations of coercivity (H_c) with temperature (T) for the powders having various crystallite sizes. The filled symbols correspond to H_c in the upper branches (H_{cu}) of the field-cooled hysteresis loop, and the open symbols to H_c in the lower branches (H_{cl}). Inset: Field-cooled (FC) and zero-field-cooled (ZFC) hysteresis loops for the 9.5-nm powder measured at 5 K and 50 K.

In Fig. 6 the temperature dependence of coercivity (H_c) is shown for various values of D; H_c was determined from the hysteresis loop ($|H| \leqslant 50$ kOe) measured after cooling the sample from room temperature in 50 kOe (FC hysteresis loop). It can be seen that H_c increases with decreasing temperature regardless of D; that the temperature dependence becomes very strong at low temperature, particularly for a smaller D; and that H_c in the upper branch (H_{cu}, filled symbols) is greater than H_c in the lower branch (H_{cl}, open symbols) at low temperatures. The last feature is seen clearly in the FC hysteresis loop of the 9.5-nm powder at 5 K, pre-

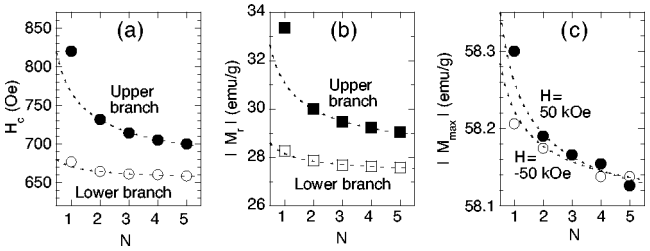

FIG. 7. Variations of (a) coercivity (H_c), (b) remanent magnetization ($|M_r|$), and (c) magnetization at $H=\pm 50$ kOe, ($|M_r|$), with the number of consecutive hysteresis-loop measurements (N), at 5 K for the 9.5-nm powder. The dotted lines are best fits of the equations $H_c=H_{c,\infty}+\alpha N^{-1/2}$, $|M_r|=|M_{r,\infty}|+\beta N^{-1/2}$, and $|M_{max}|=|M_{max,\infty}|+\gamma N^{-1/2}$ to the data points for $N\geq 2$.

sented in the inset of Fig. 6. The hysteresis loop is asymmetric so that $H_{cu}>H_{cl}$. Such an asymmetric hysteresis loop, also observed in $NiFe_2O_4$ nanoparticles,[10,11] is typical of exchange-coupled systems.[18] By contrast, the hysteresis loop measured after cooling the sample in zero field [zero-field-cooled (ZFC) hysteresis loop] is roughly symmetric. Asymmetry in the FC hysteresis loop becomes less pronounced as the temperature increases, and at 50 K the FC hysteresis loop essentially coincides with the ZFC hysteresis loop.

The observations described above are consistently explained in terms of exchange coupling between the spins in the ferrimagnetic core and those in the spin-glass shell.[11–13] The spins in the shell with multiple configurations become frozen below the spin-freezing temperature, $T_f\approx 50$ K, as is evidenced in Fig. 5(c). This makes coherent rotation of the core spins more difficult, owing to their exchange coupling with the shell spins, thereby increasing H_c. Cooling in a field establishes a shell-spin configuration for which magnetization of the core parallel to the field is energetically favorable, resulting in exchange bias and hence a hysteresis-loop shift. These effects are stronger for a smaller D because of the greater fraction of the spins lying at the core-shell interface.

There is a feature in the low-temperature FC hysteresis loops that cannot be explained by the exchange-bias effect alone: the FC hysteresis loop at 5 K (inset, Fig. 6) is not just shifted toward negative H, but the remanent magnetization (M_r) is significantly enhanced in the upper branch. [$|M_r|$ is greater in the upper branch than in the lower branch even after the hysteresis loop is shifted to the right by $H_E=(H_{cu}-H_{cl})/2$.] It is found, furthermore, that H_c, $|M_r|$, and $|M_{max}|$ (M_{max} is the magnetization at $H=\pm 50$ kOe) decrease with increasing number of consecutive measurements (N), as can be seen in Fig. 7, where H_c, $|M_r|$, and $|M_{max}|$ are plotted as functions of N. The variations of H_c and $|M_r|$ with N (≥ 2) are reasonably well described by $H_c=H_{c,\infty}+\alpha N^{-1/2}$ and $|M_r|=|M_{r,\infty}|+\beta N^{-1/2}$ for both the upper and lower branches,[26] whereas H_c and $|M_r|$ for $N=1$ are anomalously large, especially in the upper branch. Fits of the above equations to the data points for $N\geq 2$ give $H_{c,\infty}=644$ Oe and $|M_{r,\infty}|=27.3$ emu/g for the upper branch and $H_{c,\infty}=649$ Oe and $|M_{r,\infty}|=27.1$ emu/g for the lower branch. The variation of $|M_{max}|$ with N (≥ 2) roughly follows a

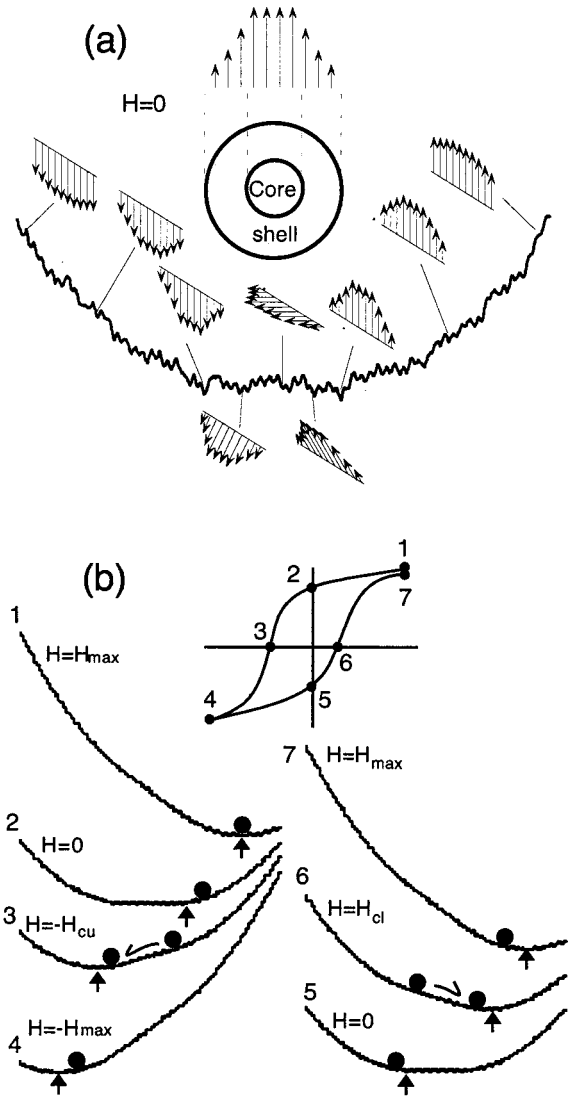

FIG. 8. (a) Schematic energy-level diagram ($H=0$) for a particle containing a ferrimagnetic core and a spin-glass shell. The arrows indicate local magnetization across the diameter of the particle. $M=M_s$ is assumed for the core. (b) Schematic energy-level diagrams under various H. The vertical arrows indicate the energy minima, while the dots denote the metastable states realized at various points (1–7) of the hysteresis loop.

similar relationship, $|M_{max}|=|M_{max,\infty}|+\gamma N^{-1/2}$, and fits of the equation to the data points yield $|M_{max,\infty}|=58.03$ and 58.07 emu/g for $H=50$ and -50 kOe, respectively. The asymptotic values of H_c and $|M_r|$ for the upper and lower branches, as well as those of $|M_{max}|$ for $H=\pm 50$ kOe, are nearly the same, suggesting a symmetric, steady-state hysteresis loop for $N=\infty$.

We provide a qualitative explanation of the decreases in H_c, $|M_r|$, and $|M_{max}|$ with increasing N using schematic energy-level diagrams for a nanoparticle presented in Fig. 8. [The arrows in Fig. 8(a) indicate local magnetizations across the diameter of a particle.] As already mentioned, ground-state spin configurations in $H=0$ would be ones in which the spins are almost random ($M\approx 0$) at the surface and gradually recover collinear ferrimagnetic arrangement ($M=M_s$) with

increasing distance from the surface, e.g., the spin configurations corresponding to the five distributions of M at the center of Fig. 8(a). (Neglecting the magnetocrystalline anisotropy energy, which is much smaller than the exchange energy, the five configurations and any other configuration obtained by coherent spin rotation are degenerate.) Those spin configurations in which the shell has a larger $|M|$ will have higher energies because of increased exchange energies in the shell. Different spin configurations are separated by a hierarchy of energy barriers associated with the spin states in the shell, with the highest barrier being of the order of $T_f \approx 50$ K.[28] The energy level diagram for the system will thus be described by a flat-bottom potential well having minor irregular modulations, as illustrated in Fig. 8(a).

Under magnetic fields, the energy-level diagram is modified as shown schematically in Fig. 8(b): a positive (negative) H lowers the energy of a spin configuration corresponding to a positive (negative) M. The spin configuration at the start of a FC hysteresis loop, which is established by cooling the sample in the maximum field (H_{max}), is in equilibrium having the lowest energy [state 1 in Fig. 8(b)]. As H is reduced, the energy minimum shifts to the left, corresponding to a spin configuration having a smaller M. Because of the presence of energy barriers, however, the spin configuration realized will be one having a larger M than in equilibrium. (Since lower energy barriers are overcome by thermal activation, M will be time dependent.) At $H=0$, the state remains to the right of the right edge of the flat bottom of the potential well, resulting in an enhanced M_r (state 2). Magnetization reversal occurs when a sufficiently high negative H is applied so that the energy barriers are lowered to values comparable to the thermal energy (state 3). State 4 at $H=-H_{max}$ will have a smaller $|M|$ than state 1, since the energy barriers prevent the establishment of an equilibrium spin configuration, which would only be achieved by cooling the system in $H=-H_{max}$. The process along the lower branch of the hysteresis loop (4,5,6,7) is similar to that in the upper branch: the potential minimum shifts to the right as H increases and a state having a smaller M than in equilibrium is realized at each H. However, $|M_r|$ and H_c will be smaller than in the upper branch because the return loop starts with a state having a larger M (smaller $|M|$). The hysteresis loop is completed with state 7, which has a smaller M than state 1. In the subsequent hysteresis-loop measurements H_c, $|M_r|$, and $|M_{max}|$ will progressively decrease because of the energy barriers, which provide ''friction'' and decrease the amplitude of the oscillation of the state in the potential well. A steady-state, symmetric hysteresis loop is established for $N=\infty$. The process of repeated field cycling is analogous to forced oscillation with a damping term.

At temperatures above T_f, the thermal energy becomes comparable to or greater than the energy barriers separating different spin configurations. This allows an equilibrium spin configuration to be realized at any H and the hysteresis loop will be symmetric and history independent.

IV. CONCLUSIONS

$MnFe_2O_4$ nanopowders ranging from 9.5 to 40 nm in crystallite size (D) have been synthesized by MCP, involving high-energy ball milling of $FeCl_3$ and MnO. Magnetic measurements on the powders (in the form of cold-pressed pellets) have revealed the following features: (i) the spontaneous magnetization (M_s) is smaller than M_s of bulk $MnFe_2O_4$ and decreases with D; (ii) the magnetization (M) vs temperature (T) curve measured in a low field of 10 Oe exhibits a kink at about 50 K, indicative of spin freezing; (iii) below about 50 K the coercivity (H_c) increases sharply with decreasing temperature, and the field-cooled hysteresis loop becomes asymmetric with enhanced H_c and remanent magnetization (M_r) in the upper branch; and (iv) H_c, $|M_r|$, and $|M|$ at the maximum $|H|$ (± 50 kOe) decrease and the asymmetry of the hysteresis loop becomes less pronounced with increasing number of consecutive hysteresis-loop measurements. These observations are consistently explained in terms of a model in which each crystallite is assumed to consist of ferrimagentic core and a spin-glass shell that are exchange coupled.

From the D dependence of M_s, the thickness of the spin-glass shell has been estimated at 9.5 Å; this value is too large to be accounted for by the distribution of exchange fields due to broken exchange bonds at the surface and surface anisotropy. We suggest that extra anisotropy and a distribution of exchange fields, and the resultant spin disorder, arise not only from the variation in the coordination number, which is limited to the cations *at* the surface, but also from the variation in the Madelung potential and the electric field set up by surface charges, which extend to the region *near* the surface.

It is found that the M vs T curves measured in a high field of 10 kOe, when normalized, are nearly independent of D indicating that unlike $MnFe_2O_4$ nanopowders prepared by wet-chemical methods, the degree of inversion does not change appreciably with D. This is a great advantage of MCP in synthesizing nanopowders for use in the study of size effects as the magnetic properties of spinel ferrites, in general, depend on the degree of inversion.

[1] T. Sato, IEEE Trans. Magn. **6**, 795 (1970).
[2] J.M.D. Coey, Phys. Rev. Lett. **27**, 1140 (1971).
[3] Z.X. Tang, C.M. Sorensen, K.J. Klabunde, and G.C. Hadjipanayis, Phys. Rev. Lett. **67**, 3602 (1991).
[4] J.P. Chen, C.M. Sorensen, K.J. Klabunde, G.C. Hadjipanayis, E. Devlin, and A. Kostikas, Phys. Rev. B **54**, 9288 (1996).
[5] K. Haneda and A.H. Morrish, J. Appl. Phys. **63**, 4258 (1988).
[6] H. Yasuoka, A. Hirai, T. Shinjo, M. Kiyama, Y. Bando, and T. Takada, J. Phys. Soc. Jpn. **22**, 174 (1967).
[7] P.J. van der Zaag, A. Noordermeer, M.T. Johnson, and P.F. Bongers, Phys. Rev. Lett. **68**, 3112 (1992).
[8] V.A.M. Brabers, Phys. Rev. Lett. **68**, 3113 (1992).
[9] P.J. van der Zaag, V.A.M. Brabers, M.T. Johnson, A. Noordermeer, and P.F. Bongers, Phys. Rev. B **51**, 12 009 (1995).

[10] A.E. Berkowitz, J.A. Lahut, and C.E. VanBuren, IEEE Trans. Magn. **MAG-16**, 184 (1980).
[11] R.H. Kodama, A.E. Berkowitz, E.J. McNiff, Jr., and S. Foner, J. Appl. Phys. **81**, 5552 (1997).
[12] R.H. Kodama and A.E. Berkowitz, Phys. Rev. B **59**, 6321 (1999).
[13] R.H. Kodama, J. Magn. Magn. Mater. **200**, 359 (1999).
[14] J.Z. Jiang, P. Wynn, S. Mørup, T. Okada, and F.J. Berry, Nanostruct. Mater. **12**, 737 (1999).
[15] J. Ding, T. Reynolds, W.F. Miao, P.G. McCormick, and R. Street, Appl. Phys. Lett. **65**, 3135 (1994).
[16] D.J. Fatemi, V.G. Harris, V.M. Browning, and J.P. Kirkland, J. Appl. Phys. **83**, 6867 (1998).
[17] O. Quénard, Ch. Laurent, M. Brieu, and A. Rousset, Nanostruct. Mater. **7**, 497 (1996).
[18] J. Nogués and I.K. Schuller, J. Magn. Magn. Mater. **192**, 203 (1999).
[19] R.S. Tebble and D.J. Craik, *Magnetic Materials* (Wiley-Interscience, London, 1969), p. 255.
[20] The formula used in Ref. 3, $M_s = M_{s0}(1-6t/D)$, results in an underestimate of t when $2t$ becomes comparable to D. In fact, a fit of this formula to our data of M_s yields $t = 7.3$ Å, a value almost the same as that derived in Ref. 3 (7 Å).
[21] On the assumption that M_s in the core ($0 \leqslant r \leqslant D/2-t$) is constant at M_{s0} and M_s in the shell ($D/2-t \leqslant r \leqslant D$) decreases linearly from M_{s0} to zero with increasing r, M_s is expressed as a function of D and t: $M_s = M_{s0}(D^3-3D^2t+4Dt^2-2t^3)/D^3$. The coefficient of the t/D term (second term) is half that of the equation we used to estimate t and D, meaning that to a first approximation the use of this more realistic model doubles the estimated value of t.
[22] J.B. Torrance, P. Lacorre, C. Asavaroengchai, and R. Metzger, Physica C **182**, 351 (1991).
[23] G.F. Dionne, J. Appl. Phys. **63**, 3777 (1988).
[24] MCP is also distinct from mechanical grinding (MG) in the following respects. First, the thermodynamics involved in the process is totally different. In MCP tiny spinel crystallites are formed directly via a displacement reaction (reaction 1), which takes place at interfaces between the two reactant phases. The free-energy change associated with the reaction is large and negative (−79 kcal/mol at 273 K), thus ensuring the formation of well-crystallized spinel structure. Ball milling does assist the reaction by continuously creating new interfaces between reactants, but the primary driving force for the spinel phase formation is the chemical energy and not the mechanical energy provided by ball milling. In MG, by contrast, small crystallites are created through progressive subdivision of larger crystals. Since the surface energy increases with decreasing D, the free-energy change associated with the process is positive, and the energy needed must be supplied in the form of mechanical energy. In other words, the process of crystal subdivision takes place only when a crystal is subjected to a sufficiently strong mechanical impact through collision events during milling. Thus, the resultant crystallites tend to be strained (Ref. 14). Second, in MCP the volume fraction of the product phase ($MnFe_2O_4$) is quite small. Even when reaction 1 is completed, the by-product phase, $MnCl_2$, accounts for 75% of the total volume. Since the reaction is far from complete during milling in the present case [Fig. 1(a)], the actual volume fraction of $MnFe_2O_4$ is still smaller. The large volume fraction of the reactant and by-product phases on the one hand significantly reduces mechanical impacts exerted on the ferrite crystals formed, and on the other prevents agglomeration of the ferrite particles. (The $MnFe_2O_4$ particles prepared by MCP are only weakly agglomerated presumably through magnetic interactions and easily broken up [Fig. 3(b)], while MG usually results in the formation of hard agglomerates.)
[25] It has been reported that cation redistribution takes place at temperatures around 400 °C in quenched bulk samples (Ref. 8) and in nanopowders prepared by coprecipitation (Ref. 4). This is not surprising, considering the presence of vacancies expected in these samples; in the former case the vacancies are entropy stabilized at the high temperature (1340 °C) from which the samples were quenched, while in the latter case cation vacancies are created because of the partial oxidation of Mn ions during crystal growth in an aqueous solution.
[26] The $N^{-1/2}$ dependence of H_c has been observed in ferromagnet/antiferromagnet bilayers (Ref. 27). The decrease in H_c with N in this case is likely related to partial orientation of the antiferromagnetic domains with each ferromagnetic magnetization reversal (Ref. 18).
[27] C. Schlenker and D. Paccard, J. Phys. (France) **28**, 611 (1967).
[28] Numerical calculations incorporating surface-spin disorder and surface anisotropy due to asymmetric atomic arrangement (Refs. 12 and 13) indeed predict an energy-level landscape consisting of higher (~20 K) and lower (~50 mK) energy barriers.